A Graph-Based Formation Algorithm for Odor Plume Tracing

Jorge M. Soares, A. Pedro Aguiar, António M. Pascoal and Alcherio Martinoli

Abstract Odor plume tracing is a challenging robotics application, made difficult by the combination of the patchy characteristics of odor distribution and the slow response of the available sensors. This work proposes a graph-based formation control algorithm to coordinate a group of small robots equipped with odor sensors, with the goal of tracing an odor plume to its source. This approach makes it possible to organize the robots in arbitrary and evolving formation shapes, with the aim of improving tracking performance. The algorithm was evaluated in a high-fidelity submicroscopic simulator, using different formations and achieving quick convergence and negligible distance overhead in laminar wind flows.

Jorge M. Soares
Distributed Intelligent Systems and Algorithms Laboratory, School of Architecture, Civil and Environmental Engineering, École Polytechnique Fédérale de Lausanne, Lausanne, Switzerland
Laboratory of Robotics and Systems in Engineering and Science, Instituto Superior Técnico, University of Lisbon, Lisbon, Portugal
e-mail: jorge.soares@epfl.ch

A. Pedro Aguiar
Department of Electrical and Computer Engineering, Faculdade de Engenharia da Universidade do Porto, Porto, Portugal
e-mail: pedro.aguiar@fe.up.pt

António M. Pascoal
Laboratory of Robotics and Systems in Engineering and Science, Instituto Superior Técnico, University of Lisbon, Lisbon, Portugal
National Institute of Oceanography, Dona Paula, Goa, India
e-mail: antonio@isr.ist.utl.pt

Alcherio Martinoli
Distributed Intelligent Systems and Algorithms Laboratory, School of Architecture, Civil and Environmental Engineering, École Polytechnique Fédérale de Lausanne, Lausanne, Switzerland
e-mail: alcherio.martinoli@epfl.ch

1 Introduction

As early as the 1950s, researchers were looking into the use of electronic devices for odor sensing, an application commonly referred to as *machine olfaction* [9, 24]. While it was not until several decades later that work in robotic olfaction began [27], it has been steadily intensifying ever since. The possibilities are endless, including very promising applications in search and rescue operations [11], as well as environmental and industrial safety [5].

Odor source localization is frequently divided in three stages: plume finding, plume traversal, and source declaration. We concentrate on the intermediate and most frequently studied, plume traversal, i.e., following a chemical plume to its source. Odor plume traversal presents particular challenges when compared to other search problems: due to turbulent transport, chemical concentration in a plume tends to be very patchy, with packets of very high concentration and periods of low or completely absent odor [26]. Along with the relatively slow response of odor sensors, this makes it hard or impractical to use simple gradient ascent techniques.

Previous work in the field has resulted in a significant number of methods for odor tracking, of which a detailed survey is provided in [14]. Many algorithms take inspiration from living creatures, such as bacteria [4] or silkworm moths [20], and generally operate by switching a single robot among a set of simple behaviors. Experiments have also been conducted with multiple robots [10, 17, 13], acting both independently and cooperatively. Other approaches include Braitenberg-type control [16], probabilistic inference [28, 17, 15] and meta-heuristic optimization methods [1, 2, 3, 12, 21].

We choose to focus on formation-based algorithms, which take advantage of multiple cooperating robots moving in formation to locate the source with minimal wandering. Our work is strongly inspired by the crosswind formation work in [18], as well as other formation- and swarm-based approaches [8, 19, 10]. This decision is driven by the choice of success metric: while the energy budget goes up with the number of robots, these techniques allow us to minimize the distance overhead and time to the source, a requirement in scenarios such as the aforementioned search and rescue. Furthermore, our solution requires very little processing power, is easy to implement, and requires no sensor information other than wind, odor and relative positions — wheel encoder information can optionally be used to improve the behavior of the algorithm.

A graph-based formation controller drives the robots to an arbitrary leaderless formation. It is based on the principle of Laplacian feedback, which has been used extensively in other contexts [22, 6]. The only information required by each robot is the relative position of its neighbors, and the formation may take an arbitrary shape and dynamically change over time. Each robot broadcasts its own odor reading, which is used to adjust the separation between robots and to bias the movement of the formation so as to center it over the plume. At all times, robots are configured with an urge to move upwind, i.e., in the expected direction of the plume source. The details of the algorithm are presented in Section 2. Note that the core of this paper is

not a specific formation proposal, but a framework that allows us to use any desired formation, possibly shaped by the underlying odor plume.

The proposed solution was validated and evaluated in a submicroscopic simulator that mimics our existing real-world infrastructure, including the Khepera III differential wheeled robots and add-on odor and wind sensing boards. The simulation arena is a model of the DISAL wind tunnel, using laminar wind flow and a filament-based odor propagation model. The fully equipped Khepera III robot and an inside view of the wind tunnel are shown in Figure 1, while Section 3 details the simulations and results obtained for two example formation shapes.

Fig. 1 (Left) Fully equipped Khepera III robot, including the range and bearing board (bottom), odor sensing board (middle) and wind sensing board (top). (Right) Inside view of the DISAL wind tunnel.

2 Controller design

Wind takes a central role in our algorithm, as odor displacement (and desired robot displacement) mostly takes place along the wind direction. Furthermore, the lack of a heading sensor renders wind our only source for global orientation.

The formation shape is specified in terms of robot positions relative to the formation center, in an *upwind - crosswind* frame, coupled with the wind direction. This allows the entire formation to rotate and align to the wind. Throughout this paper, we use the terms *forward* and *backward* to refer to the nodes respectively upwind and downwind in the desired formation. The definition of *left* and *right* of center follows naturally. The reference formation shape, as well as the relative position of each robot in it, are defined a priori and known by all robots – therefore, robots are able to independently determine which should be treated as left or forward of center.

The controller consists of a minimal set of independent behaviors: formation keeping, which drives and maintains the robots in the desired formation, upwind movement, which moves robots upwind to the source, and plume centering, which keeps the overall formation centered on the plume. Each behavior outputs a desired velocity vector, which are then combined and transformed into a control signal.

Control is distributed and asynchronous, and no supervisory information or intervention is assumed; additionally, there is no absolute positioning. Consequently, the controller operates on a local frame, in which the y axis is aligned with the robot front, pointing forward, and the x axis points 90° anticlockwise. Given the short inter-distances involved, we consider that all robots are within communication range. Nevertheless, data exchange is minimized, and the only information explicitly exchanged among the robots is the most current odor measurement.

Each behavior is described in detail in the subsequent sections. As control laws are formulated locally and homogeneous across all robots, the subscript self-identifying the node is omitted except where otherwise noted.

2.1 Sensing

Wind and odor are assumed to be measured by the sensors introduced in [17], where they are fully described. No extensive discussion of the sensor characteristics will be done in this section, as experiments took place using simulation equivalents, for which the errors models are provided in the evaluation section.

Wind measurements are provided by a custom board featuring six NTC thermistors inside individual 3D printed tubes arranged in a star shape. As wind measurements are affected by significant noise, a discrete scalar Kalman filter is used to obtain a better estimate of the relative wind direction. The wind observations are complemented by odometry information from the wheel encoders, compensating for the rotation of the robot. We consider the wind angle θ to be zero when the robot is facing the wind.

For the odor measurements, a MiCS-5521 VOC sensor is used, with a gas pump ensuring continuous flow. The sensor provides noisy quantized measurements, in the 0-1000 range. The odor readings are broadcast by each robot, along with its identification. Each robot stores the latest concentration received from every team mate, c_j, and uses it to update three values, used in the algorithm to influence the formation geometry and movement:

- c_c, the concentration measured by the center robot(s)
- c_l, the mean of concentrations measured by robots left of the formation center
- c_r, the mean of concentrations measured by robots right of the formation center

Finally, relative positions between the robots are provided by an extension board equipped with sixteen LEDs, allowing the robot to obtain the range, bearing and ID of each neighbor in line of sight [25].

2.2 Laplacian feedback

Our formation can be expressed as an undirected graph $G = (V, E)$, in which vertices V correspond to robots and edges E correspond to inter-robot relative positioning

links, or a subset thereof. From this, we can use the work in [22] and standard results in graph theory to attain a provably stable solution to the formation control problem:

$$\dot{\mathbf{x}} = -\left(\mathscr{L} \otimes I_2\right)\left(\mathbf{x} - \mathbf{b}\right) \tag{1}$$

where $\mathscr{L} = \mathscr{B}\mathscr{B}^T$ is the positive-semidefinite Laplacian matrix, obtained from the incidence matrix $\mathscr{B}$ that describes the edges of G. The (x, y) absolute position vector for all robots is given by $\mathbf{x}$, and the desired offsets to the formation centroid are given by the bias vector $\mathbf{b}$. As stated above, the law is only applicable under the assumptions of holonomicity, absolute positioning, and full connectivity maintenance.

The same approach can, however, be implemented in a decentralized fashion and using only relative positioning information, assuming a connected but not necessarily complete graph, and accounting for nonholonomicity either natively or by offloading to a lower level controller [6]. As previously discussed, we want the formation to be oriented with respect to the wind, requiring the rotation of the bias vectors by the measured wind speed θ. The resulting velocity vector for formation control is

$$\mathbf{u_f} = -\begin{bmatrix} \sum_{j=0}^{N} \mathscr{L}_j \left(x_j - \beta_j^x\right) \\ \sum_{j=0}^{N} \mathscr{L}_j \left(y_j - \beta_j^y\right) \end{bmatrix} \tag{2}$$

where $\mathscr{L}_j = \mathscr{L}_{i,j}$ is the entry of the Laplacian matrix relating the controlled node i to neighbor j, x_j and y_j are the relative positions to robot j in the body frame, and β_j is a local analogue to $\mathbf{b}$, describing the desired relative position between the two robots in the robot frame, i.e. $\beta_j = R(\theta_i)[\bar{\mathbf{p}}_\mathbf{j} - \bar{\mathbf{p}}_\mathbf{i}]$, p_i and p_j expressed in the wind/formation frame. We do not consider role assignment in this work, and so the position of each robot in the formation is defined by its ID.

2.3 Dynamic spacing

Depending on the size and growth rate of the odor plume, a fixed formation might not be an optimal choice. Therefore, we implement a method to change the formation spacing by varying the bias vector as a function of the measurements.

For simplicity, we define two scalar parameters, s_{cw} and s_{uw}, which represent adaptive bias coefficients in the crosswind and upwind direction, respectively. Assuming biases (and, hence, the formation) are symmetric, this results in a minor modification. Equation (2) remains valid, but β_j assumes a new formulation:

$$\beta_j = R(\theta_i) \begin{bmatrix} s_{cw} & 0 \\ 0 & s_{uw} \end{bmatrix} [\bar{\mathbf{p}}_\mathbf{j} - \bar{\mathbf{p}}_\mathbf{i}] \tag{3}$$

In the remainder of the paper, we choose to use a constant upwind scaling factor, and continuously vary the crosswind scaling according to (4). The underlying rationale is that, at our evaluation scale, the differences in the plume structure are more

pronounced in the crosswind direction. The scaling methods may, however, be easily modified to adapt to different realities.

$$s_{cw} = k_{cw} \frac{c_l + c_r}{1 + c_c} \tag{4}$$

Proper limits need to be set to account for the minimum safe distance and the maximum communication/movement range. We have tuned k_{cw} to approximately maintain the side robots on the detectable edges of the plume, for both the considered line and rectangular formations; values between 0.5 and 1.0 appear to yield reasonable results. However, the distribution of robots in the plume depends on its aspect ratio, strongly influenced by wind speed and other factors mediating odor dispersal.

2.4 Upwind movement and centering

While in the plume, robots should move upwind in the presumed direction of the source. Therefore, a movement urge in the direction of the apparent wind is defined:

$$\mathbf{u_w} = R(\theta) \begin{bmatrix} 0 \\ 1 \end{bmatrix} \tag{5}$$

We want to keep the formation centered in the plume, which is achieved by adding a crosswind force depending on the difference between c_l and c_r, the aforementioned means of the odor readings to the left and right of the formation center. To prevent extreme variations in control outputs due to the wide amplitude of odor measurement variations, we implement a logistic response given by

$$\mathbf{u_c} = R(\theta) \begin{bmatrix} \frac{1}{1+e^{-(c_l - c_r)/k_l}} - 0.5 \\ 0 \end{bmatrix} \tag{6}$$

The value of k_l should be approximately of the same dimension as the range of the sensor. In our experiments, $k_l = 200$. This asymptotically limits the maximum requested crosswind velocity to ± 0.5, a value that is only approached for highly asymmetric odor readings.

2.5 Behavior aggregation

We combine the requested velocity vectors of each behavior with a weighted sum

$$\mathbf{u} = k_w \mathbf{u_w} + k_c \mathbf{u_c} + k_f \mathbf{u_f} \tag{7}$$

At this stage, constant weights $k_w = k_c = k_f = 1$ are used. For the particular functions described above, this yields

$$\mathbf{u} = -\begin{bmatrix} \sum_{j=0}^{N} \mathscr{L}_j \left(x_j - \beta_j^x \right) \\ \sum_{j=0}^{N} \mathscr{L}_j \left(y_j - \beta_j^y \right) \end{bmatrix} + R(\theta) \begin{bmatrix} \frac{1}{1+e^{-(c_l - c_r)/k_l}} - 0.5 \\ 1 \end{bmatrix} \tag{8}$$

where β_j is given by (3). The resulting vector $\mathbf{u} = \begin{bmatrix} u_x & u_y \end{bmatrix}^T$ is then used to determine the requested (dimensionless) linear and angular velocities using simple proportional controllers (9) and (10), limited to forward movement and saturated a reasonable maximum within the operating range. These are passed to a motion controller that computes the actual control signals.

$$v = k_v \mathbf{u}_y \qquad 0 \leq v \leq v_{max} \tag{9}$$

$$\omega = k_\omega \mathbf{u}_x \qquad -\omega_{max} \leq \omega \leq \omega_{max} \tag{10}$$

3 Evaluation

To validate and evaluate the performance of our solution, we use a simulated equivalent of our real world wind tunnel, robots and related sensors. It is built around Webots [23], a submicroscopic robotics simulator, configured and calibrated to approximate real world behavior [17].

3.1 Setup

The simulation arena, shown in Fig. 2, is a 20 m × 4 m plane. The robots start around 14 m downwind (depending on the exact starting formation), and the source is placed at the 1 m mark, centered.

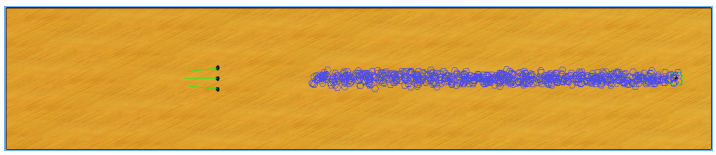

Fig. 2 Simulation setup, with the source on the right and robots starting on the left. The plume is shown in blue, and consists of filaments with growth rate $\gamma = 4 \times 10^{-7}\,\mathrm{m^2\ s^{-1}}$. The wind flows right-to-left. For ease of visualization, the filaments are drawn enlarged.

Odor propagation is modeled using filaments, and the wind flow is constant. We use the built-in model of the Khepera III, and the wind, odor and range and bearing

mechanisms are based on those available to the real robots [18]. Details of the wind and odor simulations are provided in the following subsections. Relative positioning, in the form of range and bearing measurements, is provided to the robots with angular error of 0.1 rad and range error of 10% of the distance, and is locally converted to $x-y$ coordinates.

Our simulation environment does not presently handle occlusion and always provides the range and bearing to every other robot. This is a significant limitation in the case of line formations, where occlusions are the norm. We compensate by designing the graph so that a robot only considers its two nearest neighbors in the desired formation (or just the nearest, for robots at the ends). As measurements are noisy, considering fewer neighbors leads to a less stable formation, and so our simulation underestimates expected real-world formation control performance. It also hinders the built-in collision avoidance mechanism, a problem not addressed in this work. Source declaration is outside the scope of this paper, so simulations are terminated by an external supervisor when the robots are in the vicinity of the source.

No attempt was made to maximize the robot movement speed and, consequently, minimize the mission completion time. Instead, the target speed is defined by the low-level translation of $|u_w| = 1$ into wheel speeds, and is of approximately 7 cm s^{-1}. The simulation step is of 32 ms. Communication is assumed perfect, although moderate packet loss can be tolerated with no substantial impact.

3.1.1 Wind simulation and sensing

A constant wind field of 1 m s^{-1} was used, simulating laminar flow. The wind sensor provides noisy wind velocity measurements, resulting of the sum of the (x,y,z) wind velocity at the position of the robot (w) with a vector of three independent Gaussian random variables, $N(0,\sigma_a^2)$.

As the wind field is constant, the magnitude of w is also constant and only its orientation changes. The standard deviation of the Gaussian noise is set to $\sigma_a = 0.1$ m s^{-1}. This differs from the noise distribution of the real sensor, for which the experimentally determined distribution of the *direction* noise is $N(0,\sigma_d^2)$, $\sigma_d = 4^\circ$.

3.1.2 Odor simulation and sensing

The odor propagation implementation is based on the the filament-based model proposed by Farrell et al. [7], and generates an intermittent plume similar to the one observed in the wind tunnel. Odor is simulated as a set of filaments ($i = 0,...,N$), each containing a constant amount $s = 8.3 \times 10^9$ of molecules. Each filament is defined by its (x,y,z) position $\mathbf{p}_{i,t}$, and its width $w_{i,t}$.

At each time step, the position of a filament is updated according to the wind flow and a stochastic process $\mathbf{v}_p$, consisting of a vector of three independent Gaussian random variables, $N(0,\sigma_p^2)$, with $\sigma_p = 0.1$ m. Molecular dispersion is modeled by having the filament width increase with time while the peak concentration decreases.

$$\mathbf{p}_{i,t+\Delta t} = \mathbf{p}_{i,t} + \mathbf{a}(\mathbf{p}_{i,t})\Delta t + \mathbf{v}_p \tag{11}$$

$$w_{i,t+\Delta t} = w_{i,t} + \frac{\gamma}{2w_{i,t}} \tag{12}$$

The filament dispersion rate approximating the wind tunnel conditions was previously determined to be $\gamma = 4 \times 10^{-7}$. The virtual odor source releases 100 filaments per second with an initial width of $w_{i,0} = 10$ cm and initial position distributed over the circular area of the source. The odor concentration at time t and position $\mathbf{p}$ is the sum of the concentration contribution of all filaments, which decays exponentially with the increasing distance to the center of a filament

$$c_t(\mathbf{p}) = \sum_{i=0}^{N} \frac{s}{w_{i,t}^3} \exp\left(-\frac{|\mathbf{p} - \mathbf{p}_{i,t}|}{w_{i,t}^2}\right) \tag{13}$$

No noise is added to the measured concentration as the chemical-to-electrical transduction noisy was observed to be negligible on the real platform [17]. The samples are run through a sliding window filter, which outputs the highest amongst the 50 most recent readings; in our simulation, this corresponds to a window of 1.6 s. This serves the dual purpose of emulating the approximately 1 s recovery time of the physical sensor and of adding additional noise filtering.

3.2 Results

Experiments were run for multiple formation shapes in distinct plume conditions. We provide the results for two illustrative formations: a three-robot line formation, and a five-robot rectangular formation. The results presented here are the product of single simulations, but representative of what was observed in multiple runs.

3.2.1 Line formation

The first simulation was run using a three-robot linear formation, oriented along the crosswind axis, corresponding to predefined biases $\mathbf{b}_{upwind} = \begin{bmatrix}0 & 0 & 0\end{bmatrix}^T$ and $\mathbf{b}_{crosswind} = \begin{bmatrix}1 & 0 & -1\end{bmatrix}^T$. This simulation uses a high filament growth rate $\gamma = 10^{-3}\,\mathrm{m}^2\,\mathrm{s}^{-1}$ to better highlight the adaptive formation spacing. For the same reason, the robots start centered on the plume, in close proximity - this is not a requirement, and the next section presents simulations with off-center starting positions.

Figure 3 shows the trajectories negotiated by the three robots over a total time of 180 s, overlapped with a snapshot of the simulation environment at an arbitrary time. According to the odor concentrations measured, robots begin by widening the formation and then successfully trace the limits of the plume to its source. At this scale, the trajectories appear smooth, with no major disturbances.

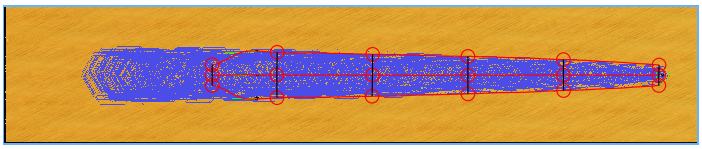

Fig. 3 Robot trajectories for a three-robot line formation in a plume with filament growth rate $\gamma = 10^{-3}\,\mathrm{m}^2\,\mathrm{s}^{-1}$. Black lines connect the robot positions at intervals of approximately 35 s.

In fact, looking at the control signals in Fig. 4, we can see that the controller is very stable in the angular speed ω, but less so in the linear speed v, which shows a standard deviation $\sigma = 0.0762$.

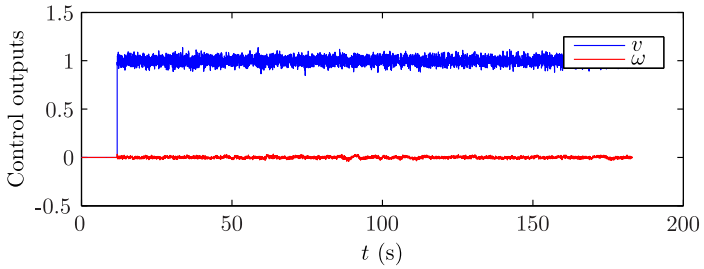

Fig. 4 Control outputs v and ω for the center robot. Both are dimensionless quantities, converted by a low level controller into the actual linear and angular speeds. The robots were parked waiting for the first nonzero odor measurements for the first 11 seconds.

Closer analysis of the results shows that, in spite of the noisy wind and odor measurements, the dominating noise present in the control outputs is introduced by the formation control, a consequence of errors in the relative positions received from the range and bearing module. Improvements could be realized by introducing a Bayesian filter for neighbor tracking, and even further by broadcasting the control outputs and wind direction estimate of each vehicle and using them to better predict future relative positions. However, the fast rate of the sensor allows us to obtain good results even in the absence of more involved strategies.

Given the central role the wind direction takes in our control law, measurement error can have a significant impact on the performance. Figure 5 shows the wind direction measurements along the complete trajectory, as well as the Kalman filter estimate of the true wind direction, a considerable improvement over the raw data.

Finally, we illustrate our statements about the intermittency of the odor plume with the recorded odor measurements from robots 1 (left) and 2 (center) in Fig. 6. While the center robot reports higher odor readings, both series show high frequency and high amplitude variation. The 50-slot sliding window maximum filter helps obtain more relevant readings, but even its output is highly noisy. Nevertheless, the

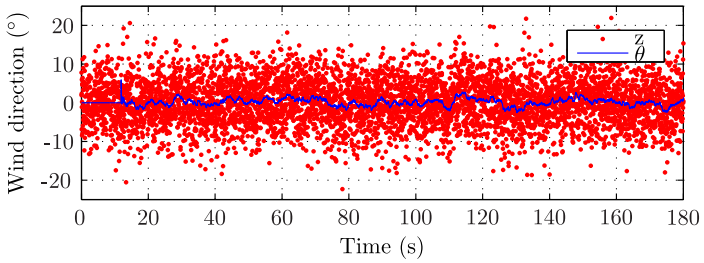

Fig. 5 Wind measurements z and Kalman estimate θ of the wind direction, relative to the front of the center robot.

logistic response in centering and relatively limited changes in formation spacing are able to minimize the impact of these variations.

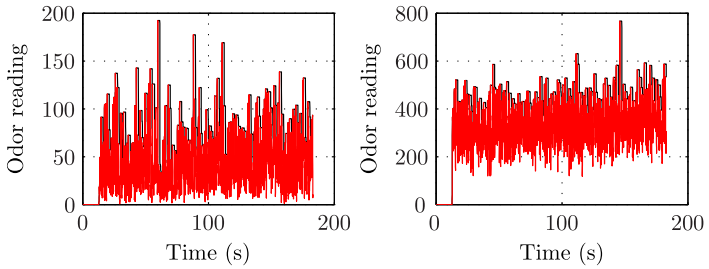

Fig. 6 Odor measurements for robots 1 (left) and 2 (center). The red lines show the instant odor measurements, and the black lines a sliding window maximum filtering. Note the different scales.

3.2.2 Rectangular formation

The rectangular formation is composed of five robots: four on the vertices and one in the center of the rear edge. This corresponds to predefined biases $\mathbf{b}_{upwind} = \begin{bmatrix}0 & 1 & 0 & 1 & 0\end{bmatrix}^T$ and $\mathbf{b}_{crosswind} = \begin{bmatrix}1 & 1 & 0 & -1 & -1\end{bmatrix}^T$. An image of the formation is provided in Fig. 7. The robots start in two clusters on the sides of the tunnel, to showcase the plume centering and formation control capabilities. Each robot is connected to the two closest neighbors along the perimeter of the formation.

In contrast to the line formation, this one introduces spatial diversity in the upwind direction. Robots along the same upwind line are able to average their readings, in order to provide the aggregate measurement c_l and c_r, less affected by individual odor packets. Figure 8 shows a 60-second plot of the readings obtained by the two robots on the left edge of the rectangle, and the resulting mean value, used as input to the controller. An additional benefit of upwind diversity, unexplored in this paper,

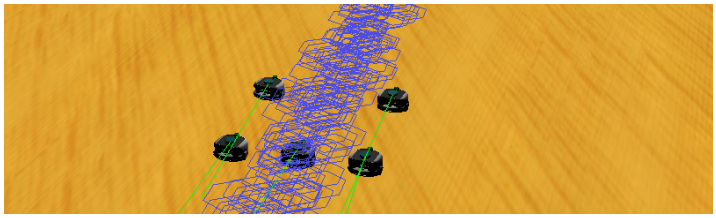

Fig. 7 Square formation. The green lines over the robots represent instant wind velocity measurements.

is the possibility of using comparatively simple formation-based source declaration mechanisms.

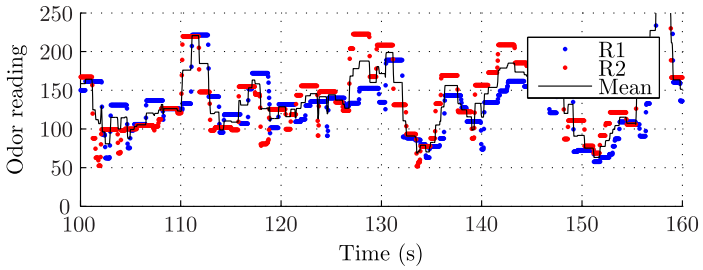

Fig. 8 Max-filtered odor measurements for robots 1 (left, back) and 2 (left, front), and resulting mean.

The trajectories followed by the robots are presented in Fig. 9. The robots converge to the desired formation and plume center in the first 30 s, and continue upwind along the target trajectory. This simulation was run with the standard filament growth rate, therefore no change in plume width is observable in this short distance.

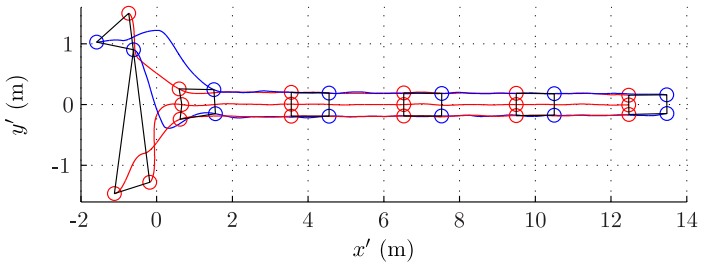

Fig. 9 Robot trajectories for a square formation in a plume with growth rate $\gamma = 4 \times 10^{-7}$. The trajectories of the forward robots are traced in blue, and those of the backward robots are traced in red. Black lines connect the robot positions at intervals of approximately 35 s.

4 Conclusions

This paper presented a formation-based controller for odor plume tracing, which uses multiple cooperating robots to trace a chemical plume to its source in laminar flow conditions. Formation control is based on Laplacian feedback and is capable of stabilizing arbitrary shapes. The formation geometry is adjusted over time to better envelope the plume, while movement is an aggregation of upwind movement and crosswind alignment.

Simulations were performed to validate the performance of the algorithm, using both a three-robot linear formation and a five-robot rectangular formation. The experiments show that the algorithm can cope with noisy readings of wind direction, odor intensity and relative positions and that, after converging to the desired positions, the robots nicely move along the centerline of the plume, tracking it to the source.

In the future, we plan to move from simulation to real-world experiments in our wind tunnel, possibly introducing Bayesian filtering on the relative positions. Afterwards, we will continue this work by further exploring the impact of different formation shapes and wind conditions through systematic experimentation.

Acknowledgements This work was partially funded by project PEst-OE/EEI/LA0009/2013 and grant SFRH/BD/51073/2010 from Fundação para a Ciência e Tecnologia. We sincerely thank Ali Marjovi at DISAL for the detailed and constructive comments.

References

1. Cabrita, G., Marques, L., Gazi, V.: Virtual cancelation plume for multiple odor source localization. In: IEEE/RSJ International Conference on Intelligent Robots and Systems, pp. 5552–5558 (2013). DOI 10.1109/IROS.2013.6697161
2. Cao, M.L., Meng, Q.H., Wang, X.W., Luo, B., Zeng, M., Li, W.: Localization of multiple odor sources via selective olfaction and adapted ant colony optimization algorithm. In: IEEE International Conference on Robotics and Biomimetics, pp. 1222–1227 (2013). DOI 10.1109/ROBIO.2013.6739631
3. de Croon, G., O'Connor, L., Nicol, C., Izzo, D.: Evolutionary robotics approach to odor source localization. Neurocomputing **121**, 481–497 (2013). DOI 10.1016/j.neucom.2013.05.028
4. Dhariwal, A., Sukhatme, G., Requicha, A.: Bacterium-inspired robots for environmental monitoring. In: IEEE International Conference on Robotics and Automation, pp. 1436–1443 (2004). DOI 10.1109/ROBOT.2004.1308026
5. Distante, C., Indiveri, G., Reina, G.: An application of mobile robotics for olfactory monitoring of hazardous industrial sites. Industrial Robot: An International Journal **36**(1), 51–59 (2009). DOI 10.1108/01439910910924675
6. Falconi, R., Gowal, S., Martinoli, A.: Graph based distributed control of non-holonomic vehicles endowed with local positioning information engaged in escorting missions. In: IEEE International Conference on Robotics and Automation, pp. 3207–3214 (2010). DOI 10.1109/ROBOT.2010.5509139
7. Farrell, J.A., Murlis, J., Long, X., Li, W., Cardé, R.T.: Filament-Based Atmospheric Dispersion Model to Achieve Short Time-Scale Structure of Odor Plumes. Environmental Fluid Mechanics **2**(1-2), 143–169 (2002). DOI 10.1023/A:1016283702837

8. Genovese, V., Dario, P., Magni, R., Odetti, L.: Self Organizing Behavior And Swarm Intelligence In A Pack Of Mobile Miniature Robots In Search Of Pollutants. In: IEEE/RSJ International Conference on Intelligent Robots and Systems, vol. 3, pp. 1575–1582 (1992). DOI 10.1109/IROS.1992.594225
9. Hartman, J.: A possible method for the rapid estimation of flavours in vegetables. Proc. Am. Soc. Hort. Sci. **64**, 335–342 (1954)
10. Hayes, A., Martinoli, A., Goodman, R.: Distributed odor source localization. IEEE Sensors Journal **2**(3), 260–271 (2002). DOI 10.1109/JSEN.2002.800682
11. Ishida, H., Nakamoto, T., Moriizumi, T., Kikas, T., Janata, J.: Plume-Tracking Robots: A New Application of Chemical Sensors. Biol. Bull. **200**(2), 222–226 (2001)
12. Jatmiko, W., Sekiyama, K., Fukuda, T.: A PSO-based mobile robot for odor source localization in dynamic advection-diffusion with obstacles environment: theory, simulation and measurement. IEEE Computational Intelligence Magazine **2**(2), 37–51 (2007). DOI 10.1109/MCI.2007.353419
13. Khalili, A., Rastegarnia, A., Islam, M.K., Yang, Z.: A bio-inspired cooperative algorithm for distributed source localization with mobile nodes. In: Annual International Conference of the IEEE Engineering in Medicine and Biology Society, pp. 3515–8 (2013). DOI 10.1109/EMBC.2013.6610300
14. Kowadlo, G., Russell, R.a.: Robot Odor Localization: A Taxonomy and Survey. The International Journal of Robotics Research **27**(8), 869–894 (2008). DOI 10.1177/0278364908095118
15. Li, J.G., Meng, Q.H., Wang, Y., Zeng, M.: Odor source localization using a mobile robot in outdoor airflow environments with a particle filter algorithm. Autonomous Robots **30**(3), 281–292 (2011). DOI 10.1007/s10514-011-9219-2
16. Lilienthal, A., Duckett, T.: Experimental analysis of gas-sensitive Braitenberg vehicles. Advanced Robotics **18**(8), 817–834 (2004). DOI 10.1163/1568553041738103
17. Lochmatter, T.: Bio-Inspired and Probabilistic Algorithms for Distributed Odor Source Localization using Mobile Robots. Phd thesis 4628, École Polytechnique Federale de Lausanne (2010). DOI 10.5075/epfl-thesis-4628
18. Lochmatter, T., Göl, E., Navarro, I., Martinoli, A.: A Plume Tracking Algorithm based on Crosswind Formations. In: International Symposium on Distributed Autonomous Robotic Systems (2010). DOI 10.1007/978-3-642-32723-0_7
19. Marjovi, A., Marques, L.: Optimal Swarm Formation for Odor Plume Finding. IEEE Transactions on Cybernetics (99) (2014). DOI 10.1109/TCYB.2014.2306291
20. Marques, L., Nunes, U., de Almeida, A.T.: Olfaction-based mobile robot navigation. Thin Solid Films **418**(1), 51–58 (2002). DOI 10.1016/S0040-6090(02)00593-X
21. Marques, L., Nunes, U., Almeida, A.T.: Particle swarm-based olfactory guided search. Autonomous Robots **20**(3), 277–287 (2006). DOI 10.1007/s10514-006-7567-0
22. Mesbahi, M., Egerstedt, M.: Graph Theoretic Methods in Multiagent Networks (2010)
23. Michel, O.: Webots: Professional Mobile Robot Simulation. International Journal of Advanced Robotic Systems **1**(1), 39–42 (2004). DOI 10.5772/5618
24. Moncrieff, R.W.: An instrument for measuring and classifying odors. Journal of Applied Physiology **16**(4), 742–749 (1961)
25. Pugh, J., Raemy, X., Favre, C., Falconi, R., Martinoli, A.: A Fast Onboard Relative Positioning Module for Multirobot Systems. IEEE/ASME Transactions on Mechatronics **14**(2), 151–162 (2009). DOI 10.1109/TMECH.2008.2011810
26. Roberts, P.J.W., Webster, D.R.: Turbulent diffusion (2002)
27. Rozas, R., Morales, J., Vega, D.: Artificial smell detection for robotic navigation. In: International Conference on Advanced Robotics, pp. 1730–1733 (1991). DOI 10.1109/ICAR.1991.240354
28. Vergassola, M., Villermaux, E., Shraiman, B.I.: 'Infotaxis' as a strategy for searching without gradients. Nature **445**(7126), 406–9 (2007). DOI 10.1038/nature05464